Remote Sensing and GIS Techniques in Hydrology

Mouhcine Batchi
University of Ibn Tofail, Morocco

Adil Moumane
University of Ibn Tofail, Morocco

IGI Global
Publishing Tomorrow's Research Today

Published in the United States of America by
IGI Global
701 E. Chocolate Avenue
Hershey PA, USA 17033
Tel: 717-533-8845
Fax: 717-533-8661
E-mail: cust@igi-global.com
Web site: https://www.igi-global.com

Library of Congress Cataloging-in-Publication Data

CIP Data Pending
ISBN:979-8-3693-9651-3
eISBN:979-8-3693-9653-7

Vice President of Editorial: Melissa Wagner
Managing Editor of Acquisitions: Mikaela Felty
Managing Editor of Book Development: Jocelynn Hessler
Production Manager: Mike Brehm
Cover Design: Phillip Shickler

British Cataloguing in Publication Data
A Cataloguing in Publication record for this book is available from the British Library.

All work contributed to this book is new, previously-unpublished material.
The views expressed in this book are those of the authors, but not necessarily of the publisher.

Table of Contents

Chapter 2
Integrating GALDIT and GIS for Assessing Sea Water Intrusion Susceptibility in the Akermoud Coastal Water Table, Morocco:
Implications for Sustainability

Abdellah Khouz
Cadi Ayyad University, Morocco & Universidade Aberta, Portugal

Jorge Trindade
Universidade Aberta, Portugal

Fatima El Bchari
Cadi Ayyad University, Morocco

Pedro Pinto Santos
https://orcid.org/0000-0001-9785-0180
University of Lisbon, Portugal

Eusébio Reis
University of Lisbon, Portugal

Adil Moumane
https://orcid.org/0000-0003-0296-2679
Ibn Tofail University, Morocco

Fatima Ezzahra El Ghazali
https://orcid.org/0000-0002-1980-3028
Cadi Ayyad University, Morocco

Mourad Jadoud
Chouaïb Doukkali University, Morocco

Blaid Bougadir
Cadi Ayyad University, Morocco

DOI: 10.4018/979-8-3693-9651-3.ch002

ABSTRACT

The Akermoud coastal aquifer, situated in the northern region of Essaouira, Morocco, is an aquifer that has an important productive capacity, mainly used for irrigation. However, uncontrolled exploitation has increased the risk of sea water intrusion, leading to deteriorating water quality and threatening agricultural sustainability. In this research, in order to access susceptibility to sea water intrusion (SWI), six elements derived from diverse databases are used. Variables were combined in a GALDIT and GIS models, resulting in the analysis of 40 groundwater samples from wells. Results highlight the imminent threat of sea water encroachment into the coastal groundwater system. The resulting GALDIT index map indicates a notably high susceptibility index along a 3 km coastal band, between Tensift Oued and Bhaybeh Beach, enlarging southwards up to 5 km. Saline intrusion patterns are particularly observed between Zaouiet El Kourati and Ouled El Fequih villages, where the merging of saline and fresh waters amplifies salinization, affecting approximately 24% of the study area.

I. INTRODUCTION

Groundwater is vital for ecosystem balance (Gholami et al., 2010; Humphreys, 2006) and is a primary water source in coastal areas (Amiri et al., 2016; Ma et al., 2020). However, groundwater quality in these regions is deteriorating, posing environmental challenges, especially in semi-arid and arid areas (Bahir and Ouhamdouch, 2020; Ez-zaouy et al., 2022; Moumane et al. 2021). Over-extraction of aquifers increases mineral content (Alabjah et al., 2018) and harms freshwater ecosystems (Mirzavand et al., 2020). Seawater intrusion, a major issue in coastal regions, is driven by groundwater recharge, discharge, and geological structure (Kumar, 2006; Seddique et al., 2019), disrupting the freshwater-seawater balance (Xue et al., 1999). Over-extraction lowers groundwater levels, triggering saline water intrusion (Pinder, 1973; Pulido-Leboeuf, 2004), which raises total dissolved solids (TDS) and renders water resources unusable (Sherif and Hamza, 2001). This issue is exacerbated by sea level rise and excessive coastal pumping (Werner and Simmons, 2009; Moujabber et al., 2006; Seddique et al., 2019).

Additional factors like agriculture (Zalidis et al., 2002), tourism (Ez zaouy et al., 2022), population density (Erostate et al., 2020), and climate change (Benini et al., 2016; Ez zaouy et al., 2022) further degrade groundwater quality in coastal regions. Salinization of coastal aquifers has garnered global attention, with various studies using models like GALDIT, coupled with hydro-geochemical analysis, to understand salinity causes and impacts (Hermans and Paepen, 2020; Ez zaouy et al., 2022).

In Morocco, population growth, economic activities, and climate change-induced rainfall decline strain water resources (Ez-zaouy et al., 2022). Uncontrolled groundwater extraction has led to unauthorized withdrawals (Laouina, 2006). The GALDIT model is effective for assessing seawater intrusion vulnerability, evaluating six key indicators (Chachadi and Lobo Ferreira, 2001; Hu et al., 2018; Ma et al., 2020). Additionally, research in hydro-geochemistry integrates major ion chemistry to analyze groundwater salinity and the fresh-saltwater interface (Han et al., 2011).

Localized studies are needed to address groundwater salinity in specific regions like the Akermoud coastal aquifers, where comprehensive investigations are lacking. Implementing preventive measures and understanding the processes controlling groundwater salinity and geochemical evolution are essential for effective management. This study integrates the GALDIT model and hydro-geochemical analysis to assess the degradation of the Akermoud aquifer under climate change and human activities, involving:

1. Assessing seawater intrusion and vulnerability using the GALDIT model.
2. Conducting a multi-approach study integrating hydro-geochemical parameters and in-situ measurements from 40 samples.
3. Evaluating groundwater quality and potential future impacts of over-extraction.
4. Enhancing the understanding of the Akermoud aquifer to develop effective management strategies.

II. GENERAL OVERVIEW OF SEAWATER INTRUSION

The chemical makeup of water plays a role in determining its usages such as drinking water, irrigation and industrial use. The quality of water and how it changes over time and across locations can be influenced by factors like the dissolution of formations as well as industrial waste and agricultural practices. Coastal underground water sources hold amounts of water for areas along the coast that are experiencing population growth and expanding agriculture, which increases the demand for water. However, there are challenges in using these resources due to issues like declining reserves and deteriorating water quality (Mdiker et al., 2009).

The Essaouira region is one area that is seeing a significant increase in its population as well as a flourishing agricultural sector. Most of the water used by the population for drinking and irrigation comes from underground sources. Seawater intrusion is a known phenomenon in regions where saltwater moves inland beneath freshwater causing significant changes in its chemistry. This has consequences on its suitability for several purposes (Fadili A., 2014).

II-1 Impact of Water Salinization on Seawater Intrusion

II-1-1 Definition of Seawater Intrusion

Seawater intrusion is an occurrence that happens when there is an inequity between the amount of freshwater and seawater. This results in a reduction of freshwater levels and an influx of seawater causing a decline in the quality of freshwater (Custodio, 2010).

II-1-2 Mechanisms of Seawater Intrusion

Coastal aquifer systems naturally discharge water towards the sea as part of the water cycle. The groundwater level in these freshwater aquifers is typically higher than the sea level, and the interface between the two is defined by a transition zone where hydrostatic equilibrium is maintained. Intensive exploitation of coastal aquifers can cause depressions that are filled by nearby seawater. Due to the density contrast between continental freshwater and saline water, seawater infiltrates the subsurface, leading to the phenomenon of seawater intrusion and subsequent degradation of water quality (Derradji, 2015).

It is evident that the coastal sector (northwestern part) of the studied region, where intensive pumping for water supply and irrigation occurs, is a vulnerable zone where the coastal aquifer is prone to saltwater contamination and direct contact with the Atlantic Ocean.

II-1-3 Transition Zone or Mixing Zone

The area where freshwater and seawater come together in aquifers is a feature. When seawater seeps into the aquifers it creates a zone where dense freshwater meets denser seawater. Over the years numerous studies have been conducted to determine the shape and location of this interface, between freshwater and seawater. Some of these studies date back to the century by researchers like Ghyben (1889) and Herzberg (1901). The thickness of this mixing zone can vary significantly ranging from a few meters to kilometers. It depends on factors such as the hydrodynamic properties of the aquifer including its permeability and diffusivity. In aquifers with hydraulic gradients this transition zone can stretch over several kilometers. Other

external factors, like tides and excessive extraction of groundwater can also impact the thickness of this mixing zone (Custodio, 2002; Fadili, A., 2014).

The phenomenon of seawater intrusion in coastal aquifers can be explained by the relationship between the freshwater head (h) above mean sea level and the depth (hs) of the freshwater-saltwater interface below sea level. This is encapsulated by the Ghyben-Herzberg equation, which can be written as:

$$\rho.(hs + h) = \rho s.hs$$

where:

- hs: depth of the interface,
- h: hydraulic head (or piezometric level) relative to the base level,
- ρ: density of freshwater,
- ρs: density of seawater.

In general, hs is approximately 40 times h.

This hydrostatic equilibrium can be altered over time. A decrease in piezometric level can lead to the intrusion of seawater into the aquifer and a difficult-to-reverse salinization.

II-1-4 Potential Sources of Freshwater Mineralization

There are two causes of freshwater salinization that can be identified;

- **Human induced salinization;** One of the reasons, for this phenomenon is the excessive extraction of groundwater compared to its replenishment rate. This issue is further exacerbated by the growth of populations in areas.
- **Natural salinization;** There are primarily two factors that influence salinization, namely geology and climate. Various chemical elements originate from rocks in the aquifer. In semiarid regions salts in water become concentrated due to evaporation. In zones salinization can occur when seawater intrudes due to limited precipitation and subsequent low recharge of the aquifer. (Fadili, A., 2014).
- **Sources of salinity in coastal aquifers;** The main cause of salinization in aquifers is seawater intrusion. However, there are contributing factors including (i) sea spray, as a source of salinity, (ii) sea level rise, (iii) evaporation and concentration of shallow water tables, (iv) dissolution of evaporites found in aquifer formations and (v) human-induced salinization. (Bear et al., 1999; Werner and Simmons 2009; Fadili, A., 2014).

II-2 GALDIT Model

Understanding the variability of aquifers regarding seawater intrusion is an essential step for his management. Numerous International literature discusses methods for evaluating vulnerability, including the GALDIT approach (Nadjla et al. 2021). GALDIT is a numerical assessment system that takes into account factors impacting the hydrogeological system. It specifically assesses the susceptibility of aquifers to seawater intrusion. This model was created by Chachadi and Lobo Ferreira (2001) within the COASTIN project a collaboration between Europe and India (Chachadi and Labo Ferreira 2005; Nadjla et al. 2021). The GALDIT method has been implemented in areas like Goa in India and Algarve, in Portugal as an index based mapping technique (Nadjla et al. 2021).

III. STUDY AREA

The focus of this chapter is on the coastal aquifer of Akermoud, situated approximately 45 km north of the city of Essaouira, Morocco. The aquifer is composed of sandstone dunes and shell limestone of the Plio-Quaternary age. It stretches along the coastline in a 20 km wide and 40 km long band (Figure 1).

Figure 1. Location of the study area

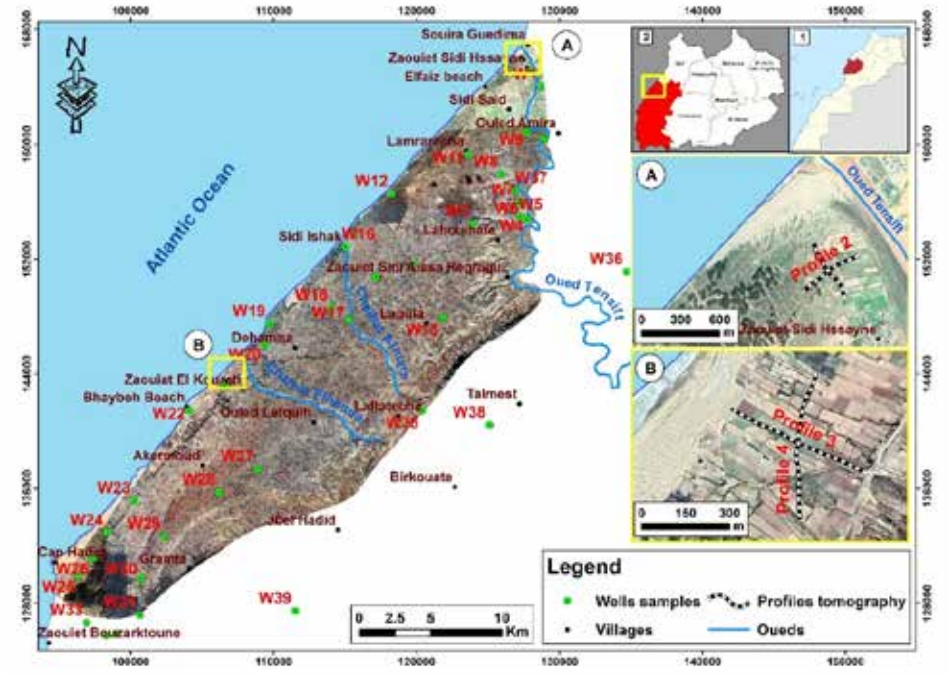

III-1 Hydrological Framework

From a hydrogeological perspective, the Essaouira basin relies heavily on a network of watercourses due to the scarcity of surface water and its limited sources. The study area is intersected by several significant rivers. The drainage basins of Oueds Chaibat Alhamra and Chaibat Almars originate from nearby mountains and the Jbel Hadid anticline, flowing into the synclinal cuvettes of the Akermoud plain (Khouz et al. 2023). These rivers tend to be short and frequently dry compared to Tensift Oued in the far north, which collects water from the High Atlas mountains.

III-2 Geological and Structural Framework

The formation of the Essaouira Basin can be attributed to the central Atlantic Rift, which initiated during the Triassic period, leading to the separation of the continents and the formation of the Atlantic Ocean. This region represents a transition from basins dominated by siliciclastic deposits to basins characterized by evaporate deposits in the Mesoproterozoic era (Salvan 1984). The Essaouira Basin, situated

between the Jbel Amsittène anticline to the south and the Jbel Hadid anticline to the north (Figure 2), is a large synclinal area that is open to the ocean. While it is influenced by various anticlinal and synclinal cuvettes individually, it is also affected by multiple tectonic events, such as the Akermoud syncline (Figure 2), located between the Atlantic Ocean and the Jbel Hadid anticline. This syncline is positioned at the center of a triangular region and marks the opening of the Akermod plain's coastal syncline (Hanich L., 2001).

Figure 2. The Akermoud plain coupe (Extracted from Monition's 1953 work)

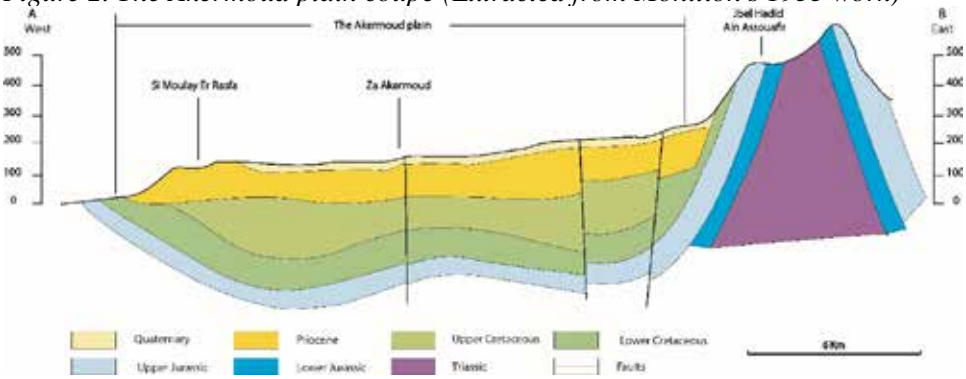

To gain a comprehensive understanding of the structure and geometry of geological formations, especially those of hydrogeological significance, a detailed study of geological data from various exploitation wells and hydrogeological reconnaissance boreholes was conducted. These data were made available to us by the ABHT and are presented in the form of descriptive sheets and lithological logs.

The well data was also used to create a geological cross-section across the entire Essaouira Basin, including the study area. The available well logs don't provide information on the ages of the encountered facies, making it impossible to establish stratigraphic correlations in terms of geological stages. Therefore, the cross-section was established through lateral facies correlation, considering three major lithological units: (i) a marl unit or predominantly marl unit, (ii) a limestone unit or predominantly limestone unit, and (iii) a suite of detrital facies encompassing silt, alluvium, dunes, etc.

The completed cross-section illustrates the deep structure of the entire Essaouira Basin to a depth of approximately 200 m. The overall shape exhibits a relatively undeformed synclinorium dominated by limestone formations with intercalated layers of marl or predominantly marl. The general picture depicted by this cross-section indicates the presence of two synclinal basins that could potentially serve as preferential zones for groundwater accumulation. The first basin, located southwest

of the cross-section, is the Meskala basin, delimited by bordering normal faults. The second basin is shallower and less pronounced, extending from the northwestern half of the basin to Jebel Hadid. The coastal zone of interest (located on the left side of the Figure 2 is characterized by the presence of significant recent overburden composed of probable Plio-Quaternary deposits. The deposition of this overburden may be related to series collapse due to normal faulting.

Due to a lack of information, the cross-section could not be extended beneath Jebel Hadid, which is known as a Triassic core anticline expected to act as a barrier between the two aquifers in our study area (Figure 2).

III-3 Hydrogeological Framework

Within the coastal plain of Akermoud, the Plio-Quaternary aquifer consists of marine or terrestrial calcite with primary hydraulic conductivity resulting from its porosity, offering a significant amount of available space. The enclosing walls of this aquifer are formed by synclinal Senonian marls. This aquifer is primarily utilized in rural areas to meet domestic water needs and other essential requirements (Bahir et al., 2000).

IV. METHODOLOGY

The methodology employed in this chapter encompasses two main axes: GALDIT modeling and hydro-geochemical approaches. By utilizing the various datasets mentioned in the Figure 3, our aim is to identify the areas most susceptible to salinization in the Akermoud water table using GIS techniques. The subsequent sections will elaborate on the methodology used for the GALDIT model and the hydro-geochemical approaches.

Figure 3. Flowchart for Marine Intrusion Methodology

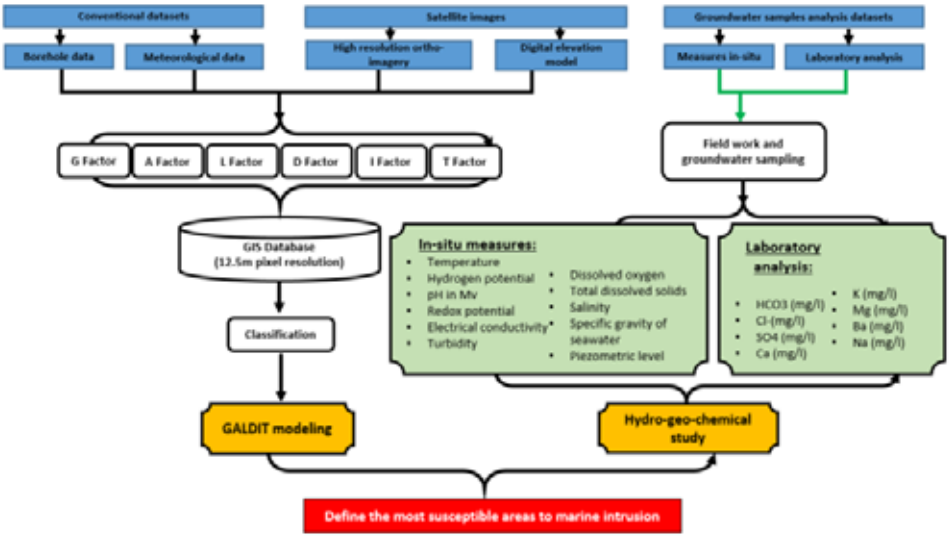

IV-1 GALDIT Modeling

The GALDIT method uses six factors related to hydrogeology, hydrology and morphology (Chachadi and Lobo Ferreira 2007) to evaluate susceptibility. These factors include the presence of groundwater (G), the aquifer's ability to transmit water (A), the groundwater level's distance from sea level (L), proximity to the shoreline (D), the impact of existing seawater intrusion (I), and the thickness of the aquifer layer (T). The significance of seawater intrusion is determined by assigning weights to each factor ranging from 1 to 4. Moreover, each factor is assigned a rating on a scale from 2.5 (indicating vulnerability) to 10 (indicating high vulnerability) as shown in Table 1.

To calculate the vulnerability index ArcGIS utilizes the raster calculator tool along, with the equation:

$$GALDIT - Index = \frac{\sum_{i=1}^{6}(W_i \cdot R_i)}{\sum_{i=1}^{6} W_i}$$

The GALDIT vulnerability index is calculated by combining the assigned ratings (R) and weights (W). The resulting index is then classified into three classes: high vulnerability (>7.5), moderate vulnerability (5 to 7.5), and low vulnerability (<5). A higher GALDIT index value indicates a greater potential for groundwater pollution and a higher vulnerability of the aquifer to seawater intrusion.

To generate the final vulnerability map, each point (borehole) is assigned a value (rating) based on Table 1. The coordinates of each borehole are used in conjunction with a GIS program to produce the map. In our study area, the hydro-geochemical parameters were obtained from sampled wells, while the other parameters were derived from the ABHT boreholes.

Table 1. Weight and ratings of the six parameters of GALDIT method

Factor	Weight	Classes	Factor variable		Rating
			Class	Range	
Groundwater occurrence/aquifer type (G)	**1**	**Class 1**	**Unconfined aquifer**		**10**
Aquifer hydraulic conductivity (Ms/l) (A)	3	Class 1	High	>9	10
		Class 2	Medium	9-6	7.5
		Class 3	Low	6-3	5
		Class 4	Very low	<3	2.5
Groundwater level above sea level (m) (L)	4	Class 1	High	<30	10
		Class 2	Medium	30–50	7.5
		Class 3	Low	50–80	5
		Class 4	Very low	>80	2.5
Distance from the shore (m) (D)	4	Class 1	High	<1000	10
		Class 2	Medium	1000–2000	7.5
		Class 3	Low	2000–6000	5
		Class 4	Very low	>6000	2.5
Impact of the existing status of seawater intrusion (I)	1	Class 1	High	>10	10
		Class 2	Medium	10–6	7.5
		Class 3	Low	6–4	5
		Class 4	Very low	<4	2.5
Thickness of the aquifer (m) (T)	2	Class 1	High	>70	10
		Class 2	Medium	70–50	7.5
		Class 3	Low	50–30	5
		Class 4	Very low	<30	2.5

The following data is required for the study:

- Inventory and coordinates of boreholes: Information and precise locations of the boreholes in the study area.

- Lithological profiles from boreholes: Detailed descriptions of the geological layers encountered in the boreholes, including the type and thickness of the aquifer.
- Depth to groundwater: Measurements of groundwater level, indicating the depth at which the water table is found.
- Hydraulic conductivity: Data obtained from pumping tests or extracted from relevant literature, providing information on the permeability of the aquifer based on its lithology.
- Topographical map: A map displaying the topography of the study area, specifically focusing on a 100-meter distance from the coastline.
- Water quality data: Data related to water quality, specifically used to calculate the Revelle coefficient (Cl/HCO_3). This information helps assess the salinity of the groundwater and its potential for seawater intrusion.

IV-2 Hydro-Geochemical Study

IV-2-1 Sampling and *In-Situ* Analysis

The work carried out in the context of this study involved sampling groundwater at 40 points distributed throughout the study area, accompanied by measurements of groundwater levels. Two field campaigns were conducted, one in 2020 (*prior* to precipitation) and another in 2021 (after direct recharge of the aquifer by precipitation). During these campaigns, the physicochemical parameters of the water were measured in situ using a HORIBA U-50 multi-parameter probe (Table 2), which provides measurements of electrical conductivity, pH, temperature, dissolved oxygen, salinity, and other parameters.

In addition to the new hydro-chemical measurements we conducted, the database provided by ABHT includes groundwater analyses conducted between 1954 and 2002. The U-50 probe used in this study simultaneously displays results for nine water characteristics parameters, namely:

- pH (Redox potential)
- DO (Dissolved oxygen)
- EC (Electrical conductivity)
- PPT (Salinity)
- TDS (Total dissolved solids)
- σT (Sea water specific gravity)
- T°C (Temperature)
- NTU (Turbidity)
- ORP(V) (Redox potential in volts)

Table 2. The specifications and typical performance characteristics of the U-50 multi-parameter probe

	Range	Resolution	Accuracy
pH	0-14	0,01pH	± 0.1pH, Automatic temperature compensation.
DO (mg/l)	0-50 mg/l	0,01 mg/l	0 à 20 mg/l ± 0.2 mg/l, et 20 à 50 mg/l ±0.5 mg/l
EC (ms/cm)EC (ms/cm)	0-9,99 S/cm	0,001 à 0,1 mS/cm	± 1% from full scale
PPT	0-70 ppt	0,1 ppt	± 3%
TDS (g/l)	0-100 g/l	0,10%	± 5 g/l.
σT	0-50 σT	0,1 σT	± 5 σ t.
T°C	-5 à 55 °C	0,01 °C	±0,15°C
NTU	0-1000 NTU	0,1 NTU	±2% of reading or 0,3 NTU
ORP (mV)	± 1999 mV	1 mV	± 15 mV.

Operational Procedure of the HORIBA U-50 Multi-Parameter Probe:

The HORIBA U50 multi-parameter probe, a water quality analyzer, consists of two components: a control unit and a probe that houses the various sensors (Figure 4).

Figure 4. Components of the HORIBA U-50 Multi-Parameter Probe

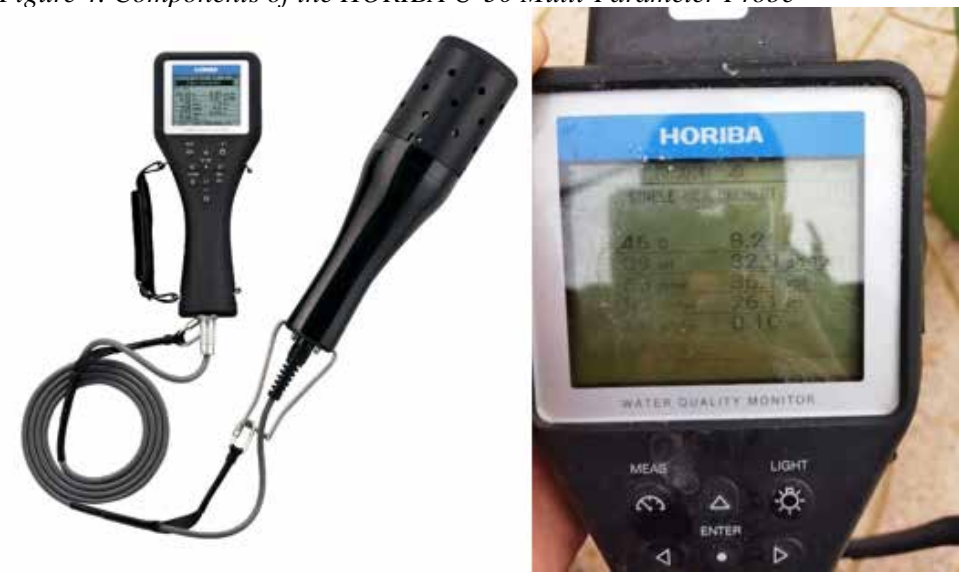

The operational procedure involves:

- Submerging the probe sensor into the water and waiting for the parameters to stabilize.
- Once the parameters have stabilized, initiating the measurement.
- The data for all the measured parameters are recorded in the device's memory and can be transferred to a computer later via a cable.

In addition to the hydro-chemical analysis, we conducted piezometric measurements using the manual piezometric probe from the Department of Geology at the Faculty of Sciences and Techniques, University Cadi Ayyad, in Marrakech. This probe is used to measure the water depth in wells, boreholes, reservoirs, etc. When the piezometric probe reaches the water surface, it emits an audible signal, and the depth reading can be observed on the graduated tape (Figure 5).

Figure 5. Examples of some wells measuring piezometric level

The collected samples were filtered first as illustrated in the Figure 6 before doing the laboratory analysis to eliminate suspended matter.

Figure 6. The samples filtration

IV-3 Laboratory Analysis

IV-3-1 Alkalinity

The alkalinity of water refers to its ability to neutralize acids. In water, alkalinity is mainly connected to carbonates, bicarbonates and hydroxides. Measuring alkalinity using the titration method involves observing the decrease in pH that happens during the determination process. To determine the alkalinity in samples, from both basins, a 0.02 N sulfuric acid solution (H_2SO_4) was used for titration (Rodier 2009).

$$CO_3^{2-} + H^+ \rightarrow HCO_3^-$$

$$HCO_3^- + H^+ \rightarrow H_2CO_3$$

During titration, the pH slightly decreases. When the sample contains carbonates, an initial equivalence point can be observed around pH 8.3. This point corresponds to the conversion of carbonate and bicarbonate ions. The endpoints can be determined using the color indicators used, such as methyl orange and phenolphthalein (Rodier 2009).

The concentrations are then visualized in mg/L, based on simple calculations involving the different volumes and equilibrium concentrations.

IV-3-2 Sulfate Determination by Nephelometry

Sulfates are commonly found in natural water bodies. Their concentrations can vary depending on factors such, as the makeup of the area or potential sources of contamination. There are techniques to determine sulfate levels, all of which rely on the formation of insoluble barium sulfate ($BaSO_4$). In this study the nephelometric method was used to measure the turbidity of the solution indicating the amount of $BaSO_4$ formed. This method involves precipitating sulfates in an environment, as barium sulfate as shown by the reaction;

$$BaCl_2 \rightarrow Ba^{2+} + 2Cl^-$$

$$Ba^{2+} + SO_4^{2-} \rightarrow BaSO_4$$

The obtained precipitate is stabilized using a Tween 20 solution. The homogeneous suspensions are measured using a UV spectrophotometer.

It is necessary to prepare calibration solutions with known sulfate concentrations in order to establish a calibration curve. This curve will allow us to determine the SO_4^{2-} content in mg/L.

The calibration curve (Figure 7) showed a high correlation coefficient (R^2 = 0.99), indicating the reliability of the standards and the results.

Several samples exhibited absorbances exceeding the range threshold (0.16), requiring multiple dilutions, especially for samples affected by seawater intrusion (dilutions up to x20).

Figure 7. Calibration curve for sulfate determination

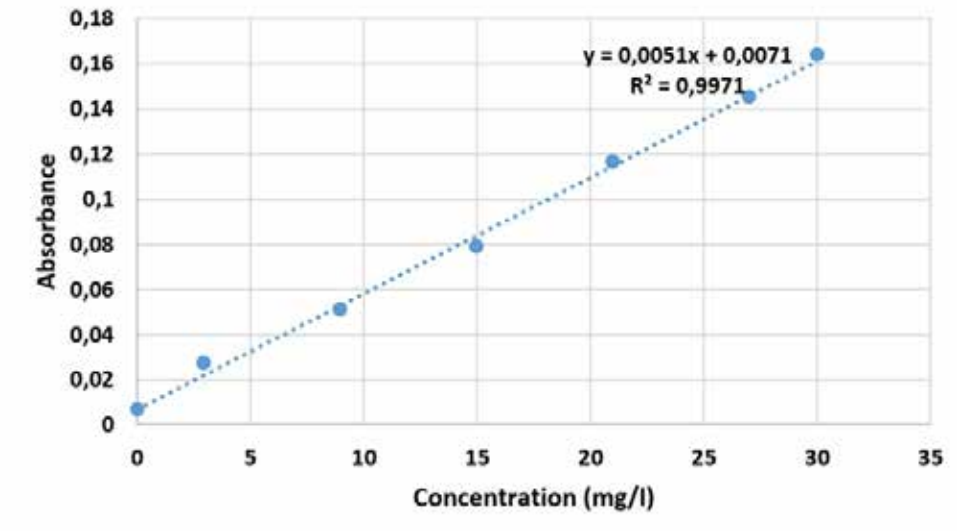

IV-3-3 Chloride Determination by Titration

The Mohr method involves precipitation titration with a solution of chloride ions of unknown concentration. After adding the potassium chromate indicator, the solution is titrated with a silver nitrate solution.

With each addition of silver ion, a precipitate of silver chloride is formed, and the solution turns red to visualize the equivalence between Ag and Cl (Rodier 2009).

$Ag^+ + Cl^- \rightarrow AgCl$ (solide)

The concentrations are then visualized in mg/L using simple calculations involving the volumes and concentrations at equilibrium.

IV-3-4 Sodium and Potassium Determination by Atomic Absorption Spectrometry

This method provides high precision and is more sensitive than flame spectrophotometry.

The solution is atomized either in a flame or in a graphite furnace at estimated temperatures of 2800°C, where it is transformed into atomic vapors. These vapors are exposed to radiation characteristic of the elements to be determined, produced by a source typically a hollow cathode lamp containing the element of interest. The radiation is absorbed by the unexcited atoms along the path of light. The concentrations are expressed in mg/L (Rodier 2009).

IV-3-4 Barium, Calcium, and Magnesium Determination by Atomic Absorption Spectrometry

Most atomic emission devices include a plasma torch (ICP torch) as this device is well suited for samples in aqueous solution. The sample, in the form of an aerosol produced by a nebulizer, is introduced at a constant flow rate of a few mg/min at the base of the torch through another small-diameter tube (1 to 2 mm). The chosen location for "light collection" from the plasma (transverse or end-on, also known as radial or axial) depends on the element and whether the analysis is based on the study of an ionic or atomic line. The temperature can range from 9,000 to 2,000 K.

IV-3-5 Ionic Balance

The ionic balance is an essential analytical tool for evaluating the quality of chemical analyses of water, and it is calculated using a simple formula:

I.B. = (Σ (cations) - Σ (anions) / Σ (cations) + Σ (anions)) x 100

The quality of the analyses is evaluated based on the following percentages:

- -5% < I.B. < 5%: Good analyses
- I.B. < ±10%: Acceptable analyses
- I.B. > ±10%: Suspicious analyses

IV-3-6 Preparation of Input Parameters

The susceptibility to Sea Water Intrusion (SWI) was evaluated using the GALDIT model, which incorporates six key parameters derived from various data sources, as illustrated in Figure 3. The Digital Elevation Model (DEM) with a 12.5 m resolution was obtained from the Alaska website.

The aquifer type (G) and thickness map were developed based on field surveys and extensive well-log profiles from the Akermoud aquifer, provided by ABHT. The hydraulic conductivity (A) of the aquifer was mapped using in-situ measurements. The groundwater depth (GW) for the Akermoud coastal aquifer was calculated by integrating static groundwater levels with topographic altitude data, collected in 2021 from 40 monitoring wells and piezometers. This data was then interpolated to provide a smooth representation of average groundwater levels.

The distance from the shore (D) was determined using Euclidean distance calculations. To evaluate the current status of SWI (I), samples from 40 groundwater boreholes and wells were analyzed. Additionally, electrical conductivity (EC) data from 16 samples were used to validate the GALDIT groundwater susceptibility model. The thickness data (T) were extracted from various well log reports.

ArcGIS Pro was employed to systematically process and prepare the thematic layers. The spatial data were georeferenced to the Lambert metric projection, zone: 1 Merchich datum. Each parameter was assigned attributes, including ratings and weights, based on their relevance to SWI. The GALDIT index was calculated using the ratings and weights recommended by Chachadi and Lobo-Ferreira (2001), considering the local hydrogeological conditions.

V. RESULTS AND DISCUSSION

V-1 GALDIT Model

V-1-1 The Akermoud GALDIT Index Parameters

Figure 8 shows the six thematic maps used to compute the GALDIT SWI susceptibility index:

- (G) - Groundwater Occurrence/Aquifer Type: The type of aquifer significantly affects the extent of SWI in freshwater. Aquifers can be classified as bounded, leaky confined, unconfined, or confined (Parizi et al., 2019; Zghibi et al., 2022). Confined aquifers with large piezometric cones due to excessive groundwater pumping are more susceptible to SWI. The Akermoud aquifer,

in this case, is unconfined with an average thickness ranging from 20 to over 100 meters, consisting mainly of sand, sandstones, and conglomerates within Quaternary deposits (Figure 8).

- (A) - Aquifer Hydraulic Conductivity: The hydraulic conductivity was converted into a raster grid and weighted appropriately. In the Akermoud area, high hydraulic conductivity zones, exceeding 9 m/day, are found along the coastal strip and near the Tensift river (Figure 8). These areas, characterized by Quaternary alluvial plains with high sand or fine sandstone content, are particularly vulnerable to SWI. In contrast, southern and eastern parts of the study area have lower permeability values (0–6 m/day), indicating reduced SWI susceptibility, with formations of Cretaceous and Jurassic origin.
- (L) - Groundwater Depth: The depth of groundwater is crucial for maintaining hydrodynamic pressure along the coast, which counteracts the inland progression of SWI. Shallower depths result in lower hydrodynamic pressure, increasing SWI risk. Conversely, higher water table levels reduce SWI risk. Groundwater depth, measured from mean sea level, is categorized into four classes (Table 2): <30 m, 30–50 m, 50–80 m, and >80 m. Areas with depths less than 30 meters, especially along the coast and near the Tensift river, are highly susceptible to SWI due to significant groundwater extraction for agriculture.
- (D) - Distance from Shore: This parameter measures the influence of SWI based on proximity to the shoreline. The extent of SWI diminishes as the distance from the coast increases (Zghibi et al., 2022). The D-parameter map for Akermoud is divided into four distance classes, with ratings ranging from 2.5 (low) to 10 (high). Areas within 1,000 m of the shore are most vulnerable to SWI, with a rating of 10. Offshore distances beyond 6,000 m receive a low rating of 2.5 (Figure 8). This parameter is assigned a weight of 4 in the GALDIT groundwater index due to its significance.
- (I) - Impact of Existing SWI Status (Cl^-/HCO_3): This parameter assesses the disruption of the natural freshwater/saltwater hydraulic balance in the transition zone.

Figure 8. The six layers of GALDIT parameters of Akermoud aquifer.

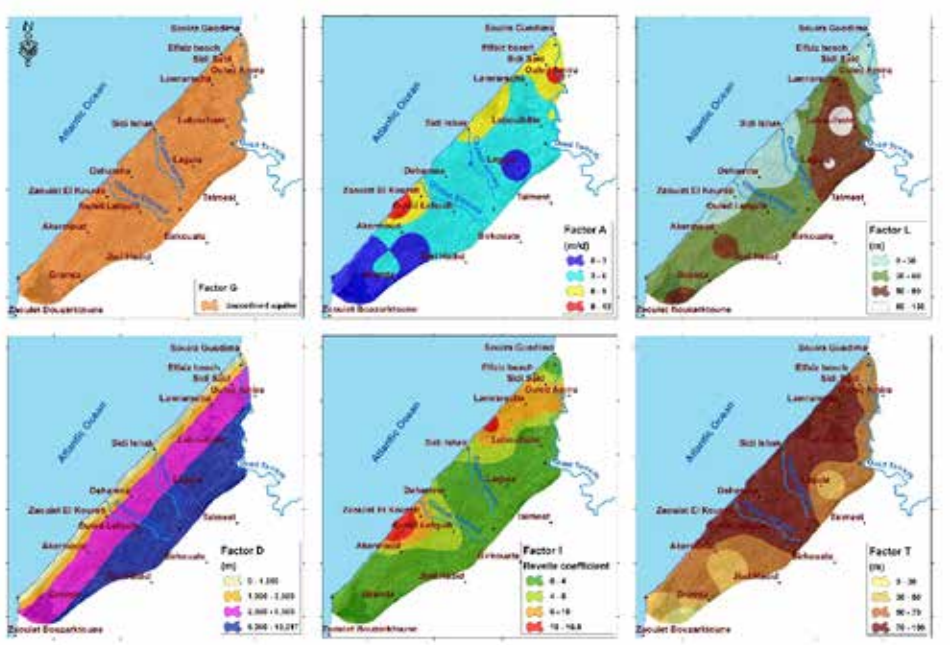

V-1-2 GALDIT GW Susceptibility Map

The GALDIT index map for the Akermoud area (Figure 9) reveals a high to very high susceptibility index, primarily observed parallel to the coastal region of the study area (discharge areas). Additionally, susceptible areas are found within a 3000-meter band inland between Tensift oued and up to 5000 meters in the southern part of Bhaybeh Beach. Further intrusion is evident between Zaouiet El Kourati and Ouled El Fequih villages, extending in an east-west direction. Notably, the Tensift Outlet experiences interference between marine and continental waters, leading to salinization of nearby wells. These vulnerable areas, characterized by sandy sandstone formations and intensive vegetable farmland, encompass approximately 24% of the study area (Table 3). This high susceptibility is attributed to multiple factors: the parameter (D) indicating a distance from the shore of less than 1 km, the parameter (I) indicating an impact of existing SWI with values above 6, the parameter (A) indicating hydraulic conductivity mostly exceeding 6 m/day, and a significant groundwater level below sea level of less than 30 meters. To ensure reliability and consistency, the results were subjected to testing and validation in subsequent analyses involving hydro-geochemical analysis.

Figure 9. Resultant SWI susceptibility maps of Akermoud aquifer

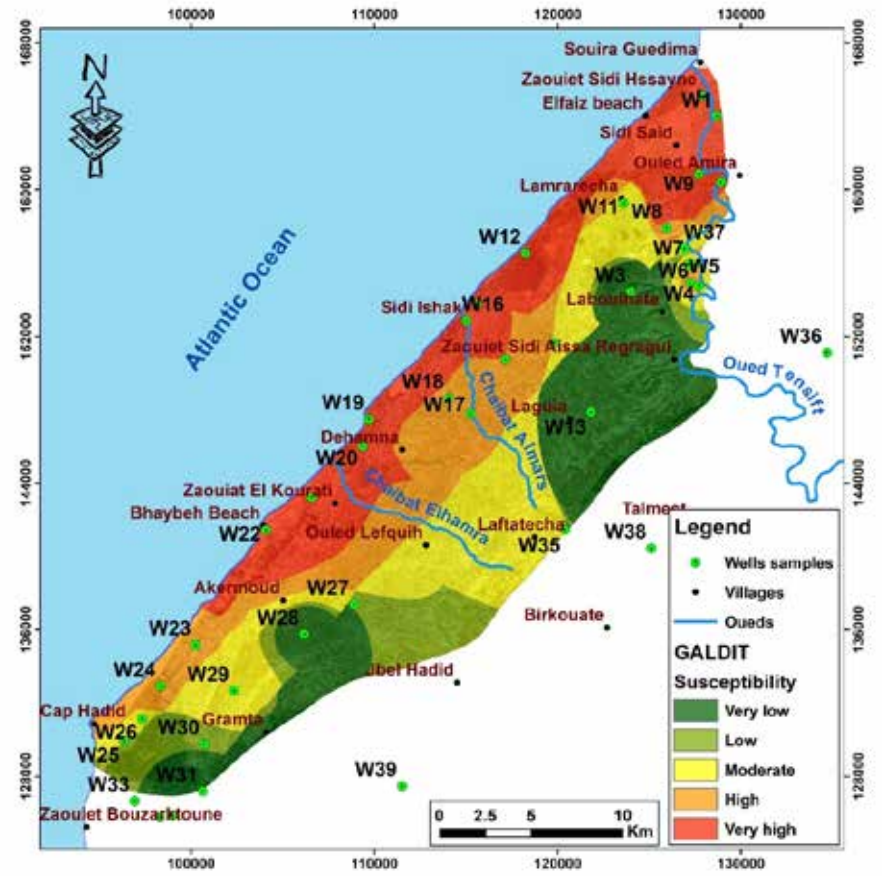

Table 3. The covered areas by the 5 classes

Susceptibility	Count pixels	Area (km²)	Percentage
Very low	709100	110.80	22.81%
Low	313466	48.98	10.09%
Medium	747336	116.77	24.04%
High	580012	90.63	18.66%
Very high	758153	118.46	24.40%

V-2 Hydro-Geochemical Contribution

The statistical analysis was conducted on 40 samples and 10 variables (EC, TDS, Ca^{2+}, Mg^{2+}, Na^{+}, K^{+}, HCO_3^{-}, Cl^{-}, SO_4^{2-}, Ba) for the Akermoud coastal aquifers situated along the Atlantic coast. To observe the spatial variation of these parameters, they were projected onto maps using GIS. Subsequently, diagrams were utilized to present the results and classify the degree of mineralization for each sample.

V-2-1 Seasonal and Spatial Variations of In-Situ Parameters

As mentioned in the methodology section, two analysis campaigns were conducted in the Akermoud aquifer: one in 2020 (before precipitation) and another in 2021 (after precipitation). There were slight differences in the sampled wells between the two campaigns, as some of them were no longer accessible. Figure 10 illustrates the spatial distribution of EC, TDS, dissolved oxygen, pH, and piezometric level for both 2020 and 2021.

For EC, which ranged from 1.36 to 9.11 in 2020 and 0.04 to 11.9 in 2021, it is worth noting that the values increased even after precipitation. This could be attributed to a greater intrusion of saline water toward the land during that year, resulting in higher EC values. Similar observations can be made for TDS, which exhibited a similar pattern of variation with different values.

Dissolved oxygen, indicating the amount of oxygen dissolved in the water, showed higher values in the northern region of Laguia and around Bhaybeh beach for both dates. The pH map, which can provide an indication of the presence of marine water or alteration of carbonic formations, revealed that pH values closer to the coastal line were more basic, with significant differences between the two dates due to variations in the sampled wells. Similarly, the piezometric level showed a change as a well located in the south of Sidi Ishak was sampled in 2020 but was no longer available in 2021.

Figure 10. Seasonal variations of in-situ measured parameters between 2020 (top row) and 2021 (bottom row)

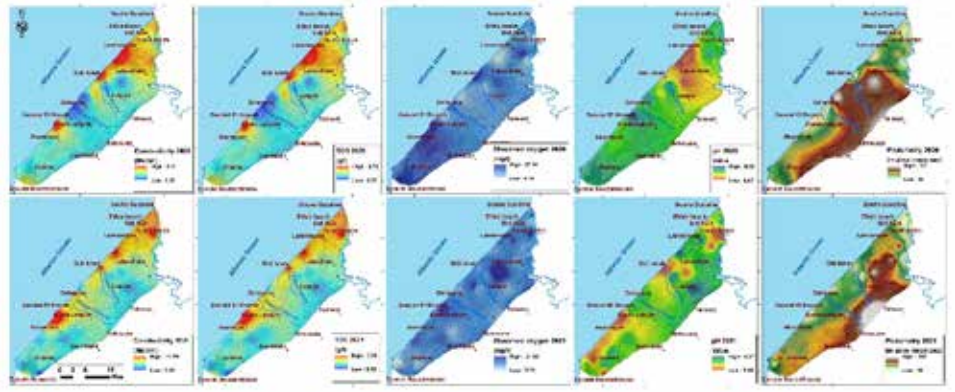

V-2-2 Spatial Variation of Laboratory Measured Parameters

After collecting water samples from the wells, various elements including Ca^{2+}, Mg^{2+}, Na^{+}, K^{+}, HCO_3^{-}, Cl^{-}, SO_4^{2-}, and Ba, were measured in different laboratories at Cadi Ayyad University. These measurements were conducted only for the second campaign, while for the first campaign, only in-situ measurements were available. Figure 11 displayed the spatial distribution of the aforementioned elements. From the Figure 11, several observations can be made:

- Bicarbonate (HCO_3), which is the predominant form of dissolved inorganic carbon in seawater and most freshwater sources, exhibited the highest values, surpassing 900 mg/l, in close proximity to Jbel Hadid. This suggests a potential lithological contamination from carbonate formations present within Jbel Hadid.
- Chloride levels, typically associated with high or elevated total dissolved solids, showed a significant increase in the Akermoud aquifer. In the northern part of the study area, after Chaibat Almars to Tensift oued, and in the south of Chaibat Elhamra around Bhaybeh beach, chloride concentrations exceeded 4500 mg/l. This indicates contamination by seawater intrusion.
- Sulfate concentrations, which should normally not exceed 250 mg/L in drinking water, exceeded 2900 mg/l near wells 11 and 17, as shown in the Figure 11 .
- Calcium, a major positive ion in natural freshwater, is widely found in minerals and constitutes 4.9% of the Earth's surface. Increased calcium concen-

trations can result from the leaching of rocks containing dissolved salts of calcium, magnesium, or iron. Groundwater in the study area receives significant calcium input from streams flowing over calcium-containing rocks and minerals found in Jbel Hadid's southern side. This explains the highest concentration of calcium between Akermoud and Zaouiat Bouzarktoune.

- Potassium (K) is one of the major components in seawater, typically present at a concentration of 380 mg/L K^+. In natural bodies of water, potassium concentrations are usually only 4% to 10% of sodium concentrations. Apart from marine contamination, the sources of potassium in the study area are likely silicate minerals, gypsum, and evaporate deposits, which release considerable amounts of potassium. This explains the higher potassium values observed in the Zaouiet El Kourati to Jbel Hadid and Lamrarecha to Tensift oued regions. Sodium (Na) is more dominant in our study area.
- Magnesium (Mg) is commonly found in groundwater that interacts with specific rocks and minerals, particularly limestone and gypsum. The dissolution of these materials releases both calcium and magnesium into the water. In our study area, magnesium mainly originates from the breakdown of dolomite, which is prevalent along Chaibat El Hamra, stemming from Jbel Hadid.
- Barium is a naturally occurring metal found in certain types of igneous and sedimentary rocks. Barium can enter groundwater and well water when rocks containing barium break down and dissolve. Barium can also combine with other chemicals to form compounds. The highest concentrations of barium are mainly located around the northern region of Jbel Hadid, suggesting potential lithological contamination.

Figure 11. Spatial variation of laboratory measured parameters (Ca^{2+}, Mg^{2+}, Na^{+}, K^{+}, HCO_3^{-}, Cl^{-}, SO_4^{2-} and Ba)

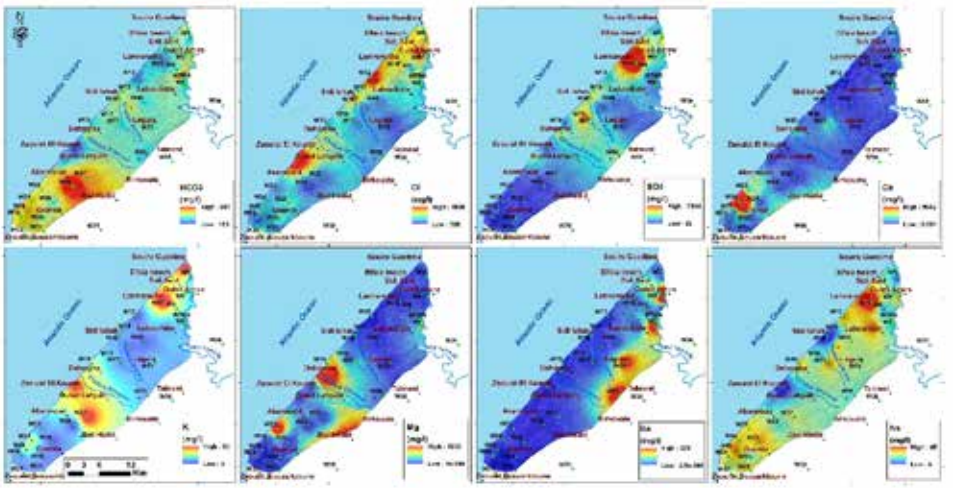

V-3 Water Classification With Conventional Diagrams

V-3-1 Piper Diagram

The results presented in Figure 12 demonstrate the dispersed distribution of samples in the piper diagrams, indicating the presence of specific hydro-chemical processes and mixing between different types of water samples. The diagrams provide insights into the groundwater characteristics of the Akermoud coastal aquifers, revealing a predominance of Ca–Cl type water followed by Na–Cl type water and mixed types.

Figure 12. Piper's trilinear diagram, illustrates the relationship between dissolved ions and water types in the Akermoud coastal aquifers

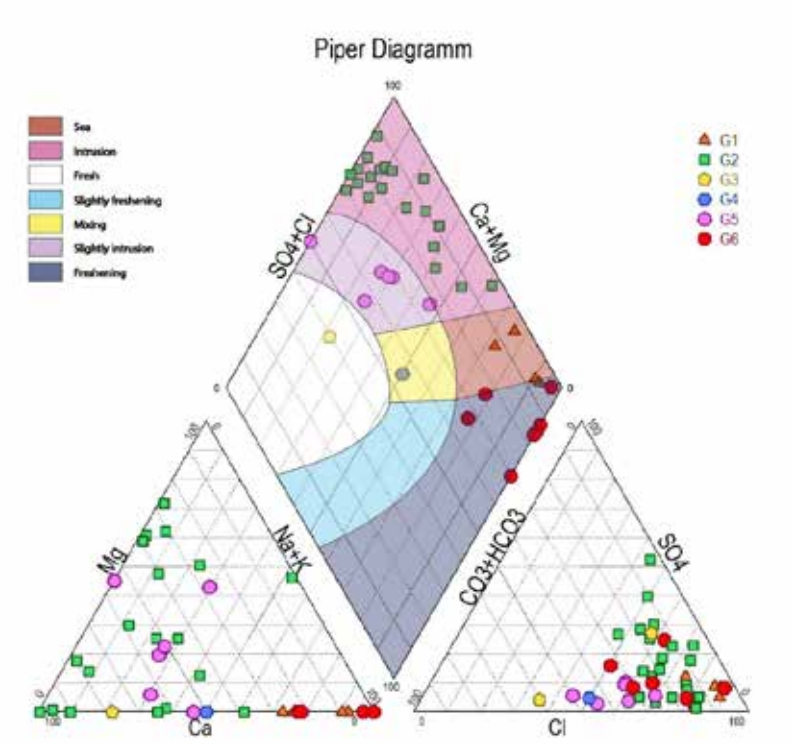

The samples were categorized into six groups:

- Sea group (G1): This group includes samples W7, W9, W12, W21, and W40.
- Intrusion group (G2): This group comprises samples W11, W33, W8, W5, W16, W18, W37, W1, W32, W6, W35, W10, W3, W19, W2, W23, W24, W4, W17, and W20.
- Fresh group (G3): Only sample W28 belongs to this group.
- Mixing group (G4): Only sample W38 falls into this group.
- Slightly intrusion group (G5): This group consists of samples W26, W25, W13, W31, W14, and W39.
- Freshening group (G6): This group includes samples W27, W22, W40, W15, W29, W30, and W34.

Based on the data presented in Figure 12, it is evident that 50% of the samples (20 out of 40) fall into the intrusion category, characterized by a predominant Ca–Cl water type. This suggests significant interaction between groundwater and saline

waters. The anion triangle plot indicates that several samples are closer to the chloride apex. However, two distinct trends emerge: one group of samples is located between the bicarbonate and chloride poles, while the other group falls between the sulfate and chloride poles. These trends can be attributed to the dissolution of geological formations and the impact of seawater intrusion, which intensifies base exchange processes.

In the cation plot, most data points are concentrated around the ($Na^+ + K^+$) zone, with the exception of point W28, which lacks a dominant cation signature. Additionally, the majority of the points are positioned above the theoretical mixing line, indicating that many of the samples have been influenced by saltwater intrusion. The water types in the study area appear to be shaped by a combination of factors, including anthropogenic activities (e.g., agriculture and groundwater overuse), surface water-aquifer interactions, and the mixing of groundwater with marine waters.

V-3-2 Gibbs Diagram

The Gibbs diagrams (Figure 13) reveal that most samples are located within the evaporation domain and the rock weathering zone, trending towards the seawater influence field. Notably, sample W31 is positioned within the rock dominance region. This pattern indicates that the groundwater chemistry in the studied aquifer is predominantly influenced by rock weathering processes, which are associated with seawater intrusion. It's important to note that nearly all samples extend beyond the Gibbs diagram boundaries, especially in terms of the $Na^+ / (Na^+ + Ca^{2+})$ ratio. This occurrence is likely due to an excess of Ca^{2+} resulting from water-rock interactions and ion exchange processes influenced by seawater intrusion (Chen et al., 2020; Liu et al., 2020). Furthermore, the $Cl^- / (Cl^- + HCO_3^-)$ ratio shows variation with increasing total dissolved solids (TDS), which may be attributed to higher Cl^- concentrations resulting from evaporation-crystallization processes (Liu et al., 2020b), sea spray, or seawater intrusion.

Figure 13. Gibbs diagram representing the ratio of $Na^+/(Na^+ + Ca^{2+})$ and $Cl^-/(Cl^- + HCO_3^-)$ as a function of TDS in Akermoud coastal aquifers.

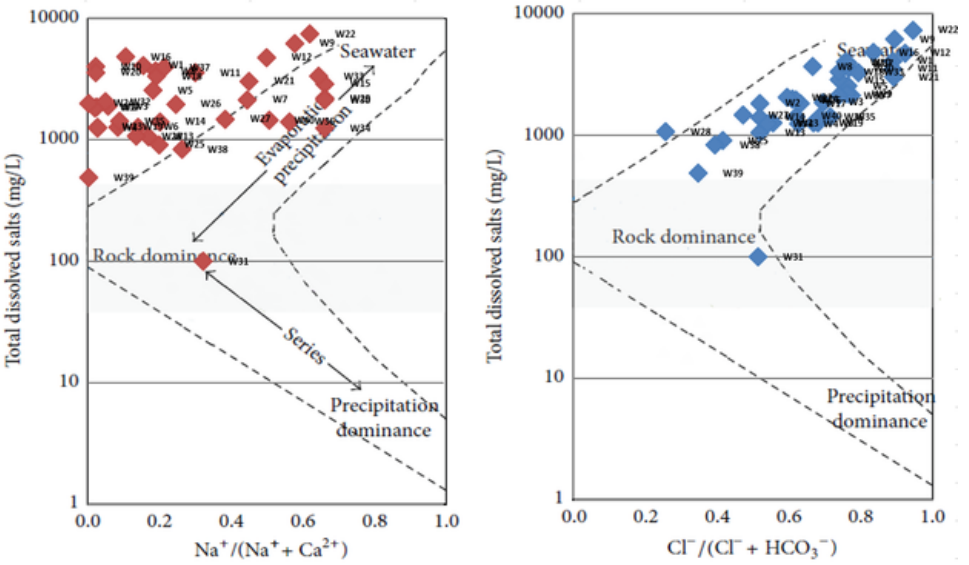

V-3-3 Sodium Absorption Ratio (SAR) and Sodium Percentage (Na^+ %)

It is important to note that, for the Wilcox graphs, we have once again categorized our samples into four groups based on their quality:

- Group 1: Includes samples W5, W7, W8, W9, W10, W11, W12, W15, W16, W18, W20, W21, W22, W24, W26, W29, W30, W32, W33, W34, W36, and W37.
- Group 2: Includes samples W2, W3, W14, W17, W27, W35, and W40.
- Group 3: Includes samples W4, W6, W13, W19, W23, W25, W28, W38, and W39.
- Group 4: Contains only sample W31.

In Figure 14, the SAR (Sodium Adsorption Ratio) values of the groundwater in the Akermoud aquifer are depicted, ranging from 0 to 5 with an average of 2. Analyzing the SAR diagrams in relation to electrical conductivity, we find that the samples fall into the following classes: C3S1, C4S1, C5S1, and C5S2 (Figure 14). These classes indicate high to very high salinity and low to medium alkalinity, suggesting that the water is unsuitable for irrigation purposes.

Figure 14. Classification of Akermoud aquifer and the groundwater suitability for irrigation purpose based on (EC and SAR).

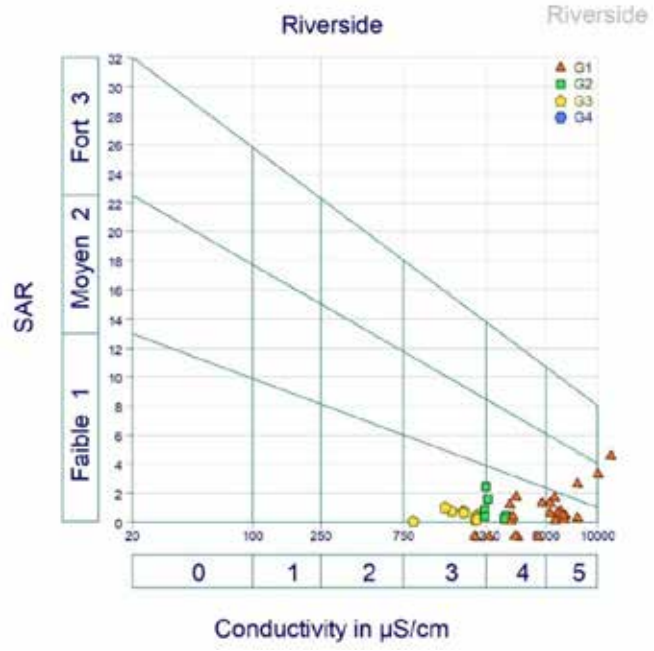

(Given that: $\boldsymbol{SAR} = \frac{\boldsymbol{Na}}{\sqrt{\frac{1}{2}(\boldsymbol{Ca} + \boldsymbol{Mg})}}$)

Additionally, in Figure 15, the Wilcox (1955) diagram presents the Na^+ % projection for the Akermoud coastal aquifers, showing a wide range of Na^+ % values from 0% to over 100%. Based on this projection, we can identify four main groups that were previously mentioned in this context. Group 1 corresponds to water of poor quality, Group 2 represents water of mediocre quality, Group 3 indicates good quality water, and Group 4 signifies excellent quality water. The majority of the water samples fall within the range of poor to mediocre quality. This situation can be attributed to an excess of sodium caused by the intrusion of seawater and water-rock interactions involving the dissolution of halite and evaporitic formations.

Figure 15. Classification of Akermoud coastal aquifer and groundwater suitability for irrigation purpose based on (EC and Na^+ %).

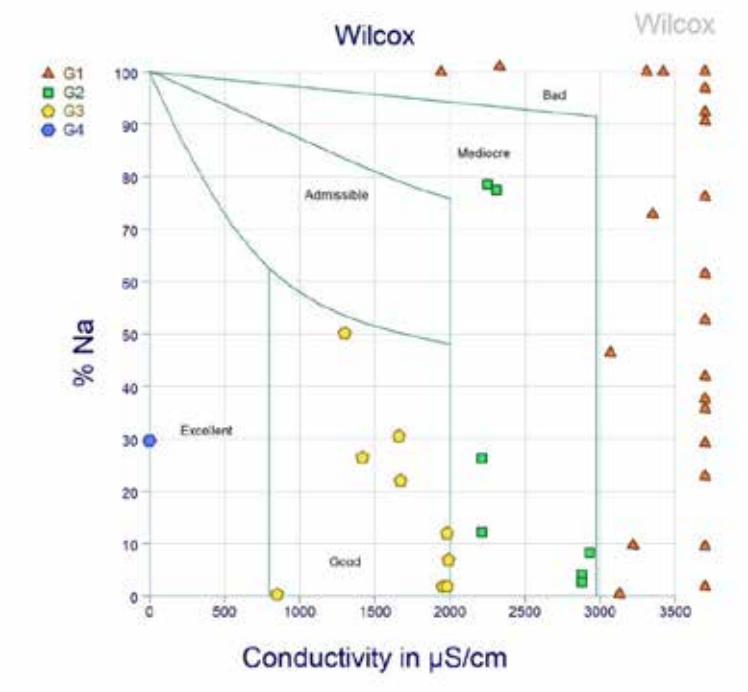

(Given that: $Na\,\% = \frac{100*(Na+K)}{(Ca+Mg+Na+K)}$)

VI. CONCLUSION

In summary, effectively managing the coastal aquifer in the Akermoud district necessitates a thorough understanding of the factors influencing groundwater salinity and geochemical changes. To this end, a combined approach of modeling and hydro-geochemical analysis was utilized to evaluate the extent of the aquifer's degradation due to climate change and human activities.

The GALDIT model was utilized to understand the encroachment and extent of seawater susceptibility into the groundwater system. The model indicated high to very high susceptibility index zones, primarily located parallel to the coast and in areas within a 3000 m inland band. Notably, the Tensift Outlet exhibited significant salinization of nearby wells due to the interaction between marine and continental

waters. These findings were further validated through hydro-geochemical analysis to ensure reliability and consistency.

A comprehensive study was conducted, involving the collection of 40 groundwater samples from different types of tubewells. These samples were then subjected to analysis using the GALDIT Model, and hydro-geochemical techniques. The combined results of these analysis revealed the presence of marine intrusion in the study area.

Notably, the groundwater samples obtained from wells in close proximity to the coast, Tensift Oued, and certain areas in the eastern part of the study area exhibited significantly high values of electrical conductivity (EC) and total dissolved solids (TDS). This indicates a clear influence of seawater on the groundwater quality in these locations. The intrusion of marine water and the presence of saline lithological formations contribute to the observed geochemical variations.

The hydro-geochemical analysis focused on major ions and total dissolved solids (TDS). The results showed that a significant portion of the samples exhibited a dominant Ca-Cl water type, indicating groundwater interaction with saline waters. The analysis also revealed the dissolution of evaporitic formations and the impact of seawater intrusion, which led to the exchange of bases. Furthermore, the cation analysis demonstrated a tendency towards the domain of Na^{++} and K^{+} for most samples, suggesting the influence of seawater intrusion. Overall, the water types in the aquifer were affected by multiple factors such as anthropogenic activities, surface water interaction, and mixing with marine waters.

Overall, this multi-approach study provided valuable insights into the state of the Akermoud aquifer, including the susceptibility to seawater intrusion, hydro-geochemical characteristics, and subsurface features. The findings emphasized the need for effective management strategies to address the current groundwater quality and potential future impacts, particularly due to overexploitation and climate change.

The consequences of such geochemical variations are profound. The quality of irrigation water, as indicated by these samples, was found to be extremely poor in approximately half of the cases. Moreover, the quality of potable water has deteriorated to a significant extent due to the effects of marine intrusion and the contribution of saline lithological formations. This poses a serious concern for both agricultural activities and access to safe drinking water.

The impact of saline irrigation water on soil structure is particularly noteworthy. The higher the salinity of the irrigation water, the greater the adverse effects on soil quality and structure. Continuous irrigation with saline water leads to the accumulation of sodium in the soil over time, resulting in diminished soil fertility and decreased crop yields. This highlights the urgent need for improved water management practices to mitigate the detrimental effects on soil and ensure sustainable agricultural productivity.

Due to the scarcity of soil resources in these regions, it is vital to encourage societal adaptation and promote behavioral changes. Moreover, the formulation of suitable management strategies is necessary to support a shift towards sustainable hydrological conditions. By embracing sustainable practices and implementing effective water management approaches, the impacts of marine intrusion can be minimized, ensuring the long-term sustainability of the hydrological system in these areas.

REFERENCES

Alabjah, B., Amraoui, F., Chibout, M., & Slimani, M. (2018). Assessment of saltwater contamination extent in the coastal aquifers of Chaouia (Morocco) using the electric recognition. *Journal of Hydrology (Amsterdam)*, 566, 363–376. DOI: 10.1016/j.jhydrol.2018.09.003

Amiri, V., Nakhaei, M., Lak, R., & Kholghi, M. (2016). Geophysical, isotopic, and hydrogeochemical tools to identify potential impacts on coastal groundwater resources from Urmia hypersaline Lake, NW Iran. *Environmental Science and Pollution Research International*, 23(16), 16738–16760. DOI: 10.1007/s11356-016-6859-y PMID: 27184149

Badon-Ghyben, W. (1889). Nota in verband met de voogenomen put boring nabij Amsterdam (Notes on the probable results of the proposed well drilling near Amsterdam). *Tijdschr. Kon. Inst. Ing.*, 8-22.

Bahir, M., Mennani, A., Jalal, M., & Youbi, N. (2000). Ressources hydriques du bassin synclinal d'Essaouira (Maroc). *Estudios Geológicos (Madrid)*, 56(3-4), 185–195. DOI: 10.3989/egeol.00563-4150

Bahir, M., Ouhamdouch, S., Ouazar, D., & El Moçayd, N. (2020). Climate change effect on groundwater characteristics within semi-arid zones from western Morocco. *Groundwater for Sustainable Development*, 11, 100380. DOI: 10.1016/j.gsd.2020.100380

Bear, J., Cheng, A. H. D., Sorek, S., Ouazar, D., & Herrera, I. (Eds.). (1999). *Seawater intrusion in coastal aquifers: concepts, methods and practices* (Vol. 14). Springer Science & Business Media. DOI: 10.1007/978-94-017-2969-7

Benini, L., Antonellini, M., Laghi, M., & Mollema, P. N. (2016). Assessment of water resources availability and groundwater salinization in future climate and land use change scenarios: A case study from a coastal drainage basin in Italy. *Water Resources Management*, 30(2), 731–745. DOI: 10.1007/s11269-015-1187-4

Chachadi A.G., Lobo-Ferreira J.P. (2001). Sea water intrusion vulnerability mapping of aquifers using GALDIT method. Proceedings of the workshop on modelling in hydrogeology, 143–156.

Chachadi A.G., & Lobo-Ferreira J.P. (2005). Assessing aquifer vulnerability to seawater intrusion using GALDIT method: part 2- GALDIT Indicator Descriptions. In IAHS and LNEC, proceedings of the 4 the fourth interceltic colloquium on hydrology and management of water resources. University Minho.

Chachadi, A.G., & Lobo-Ferreira, J.P. (2007). Assessing aquifer vulnerability to seawater intrusion using GALDIT method: Part 2, GALDIT indicators description. *Water Celt Countries Quant Qual Clim Var*, 310, 172–180.

Custodio, E. (2002). Aquifer overexploitation: What does it mean? *Hydrogeology Journal*, 10(2), 254–277. DOI: 10.1007/s10040-002-0188-6

Custodio, E. (2010). Coastal aquifers of Europe: An overview. *Hydrogeology Journal*, 18(1), 269–280. DOI: 10.1007/s10040-009-0496-1

Derradji, F. (2015). *Intrusion marine dans les nappes côtières: cas de la nappe des graviers d'Annaba*. Extrême Nord-Est d'Algérie.

Erostate, M., Huneau, F., Garel, E., Ghiotti, S., Vystavna, Y., Garrido, M., & Pasqualini, V. (2020). Groundwater dependent ecosystems in coastal Mediterranean regions: Characterization, challenges and management for their protection. *Water Research*, 172, 115461. DOI: 10.1016/j.watres.2019.115461 PMID: 31951946

Ez-zaouy, Y., Bouchaou, L., Saad, A., Hssaisoune, M., Brouziyne, Y., Dhiba, D., & Chehbouni, A. (2022). Morocco's coastal aquifers: Recent observations, evolution and perspectives towards sustainability. *Environmental Pollution*, 293, 118498. DOI: 10.1016/j.envpol.2021.118498 PMID: 34798220

Fadili, A. (2014). *Etude hydrogéologique et géophysique de l'extension de l'intrusion marine dans le Sahel de l'Oualidia (Maroc): analyse statistique, hydrochimie et prospection électrique* (Doctoral dissertation, Univérsité de Chouaïb Doukkali Faculté Des Sciences El Jadida).

Gholami, V., Yousefi, Z., & Zabardast Rostami, H. (2010). Modeling of ground water salinity on the Caspian southern coasts. *Water Resources Management*, 24(7), 1415–1424. DOI: 10.1007/s11269-009-9506-2

Han, D., Kohfahl, C., Song, X., Xiao, G., & Yang, J. (2011). Geochemical and isotopic evidence for palaeo-seawater intrusion into the south coast aquifer of Laizhou Bay, China. *Applied Geochemistry*, 26(5), 863–883. DOI: 10.1016/j.apgeochem.2011.02.007

Herzberg, A. (1901). Die wasserversorgung einiger Nordseebader. *J. Gasbeleucht. Wasserversorg.*, 44, 815–819.

Hanich, L. (2001) Structure et fonctionnement d'un aquifère multicouche carbonaté. Exemple du bassin d'Essaouira. Guide méthodologique. Thèse d'Etat ès Sciences Naturelles, Université Cadi Ayyad, Faculté des Sciences et Techniques de Marrakech, Maroc.

Hermans, T., & Paepen, M. (2020). Combined inversion of land and marine electrical resistivity tomography for submarine groundwater discharge and saltwater intrusion characterization. Geophysical Research Letters, 47(3). DOI: 10.1029/2019GL085877

Hu, J., Dong, H., Xu, Q., Ling, W., Qu, J., & Qiang, Z. (2018). Impacts of water quality on the corrosion of cast iron pipes for water distribution and proposed source water switch strategy. *Water Research*, 129, 428–435. DOI: 10.1016/j.watres.2017.10.065 PMID: 29179122

Humphreys, E. R., Lafleur, P. M., Flanagan, L. B., Hedstrom, N., Syed, K. H., Glenn, A. J., & Granger, R. (2006). Summer carbon dioxide and water vapor fluxes across a range of northern peatlands. *Journal of Geophysical Research*, 111(G4), 2005JG000111. Advance online publication. DOI: 10.1029/2005JG000111

Khouz, A., Trindade, J., Santos, P. P., Oliveira, S. C., El Bchari, F., Bougadir, B., Garcia, R. A. C., Reis, E., Jadoud, M., Saouabe, T., & Rachidi, S. (2023). Flood susceptibility assessment through statistical models and HEC-RAS analysis for sustainable management in Essaouira Province, Morocco. *Geosciences*, 13(12), 382. DOI: 10.3390/geosciences13120382

Laouina, A. (2006). Le litoral marocain, milieux côtier et marin. *Environnement et Territoires, Cadre Natural*, 187-216.

Ma, C., Li, Y., Li, X., & Gao, L. (2020). Evaluation of groundwater sustainable development considering seawater intrusion in Beihai City, China. *Environmental Science and Pollution Research International*, 27(5), 4927–4943. DOI: 10.1007/s11356-019-07311-3 PMID: 31840220

Mdiker, N. A. B. I. L., El Achheb, A., Mandour, A., Younsi, A., El Maliki, S., & Outeyeb, B. (2009). Contribution à l'étude de la salinisation de la nappe côtière de sahel El Haouzia région d'El Jadida au Maroc. *Afrique Science: Revue Internationale des Sciences et Technologie, 5*(2).

Mirzavand, M., Ghasemieh, H., Sadatinejad, S. J., & Bagheri, R. (2020). An overview on source, mechanism and investigation approaches in groundwater salinization studies. *International Journal of Environmental Science and Technology*, 17(4), 2463–2476. DOI: 10.1007/s13762-020-02647-7

Monition, L. (1953). *Sur l'intérêt de sondages dans la plaine d'Akermoud*. Rap. Inéd. MTPC/DH/DRE.

Moujabber, M. E., Samra, B. B., Darwish, T., & Atallah, T. (2006). Comparison of different indicators for groundwater contamination by seawater intrusion on the Lebanese coast. *Water Resources Management*, 20(2), 161–180. DOI: 10.1007/s11269-006-7376-4

Moumane, A., El Ghazali, F. E., Al Karkouri, J., Delorme, J., Batchi, M., Chafiki, D., & Karmaoui, A. (2021). Monitoring spatiotemporal variation of groundwater level and salinity under land use change using integrated field measurements, GIS, geostatistical, and remote-sensing approach: Case study of the Feija aquifer, Middle Draa watershed, Moroccan Sahara. *Environmental Monitoring and Assessment*, 193(12), 769. DOI: 10.1007/s10661-021-09581-2 PMID: 34735624

Nadjla, B., Abdellatif, D., & Assia, S. (2021). Mapping of the groundwater vulnerability to saline intrusion using the modified GALDIT model (Case: The Ain Temouchent coastal aquifer,(North-Western Algeria)). *Environmental Earth Sciences*, 80(8), 319. DOI: 10.1007/s12665-021-09614-6

Parizi, E., Hosseini, S. M., Ataie-Ashtiani, B., & Simmons, C. T. (2019). Vulnerability mapping of coastal aquifers to seawater intrusion: Review, development and application. *Journal of Hydrology (Amsterdam)*, 570, 555–557. DOI: 10.1016/j.jhydrol.2018.12.021

Pinder, G. F. (1973). A Galerkin-finite element simulation of groundwater contamination on Long Island, New York. *Water Resources Research*, 9(6), 1657–1669. DOI: 10.1029/WR009i006p01657

Pulido-Leboeuf, P. (2004). Seawater intrusion and associated processes in a small coastal complex aquifer (Castell de Ferro, Spain). *Applied Geochemistry*, 19(10), 1517–1527. DOI: 10.1016/j.apgeochem.2004.02.004

Rodier, J., Legube, B., & Merlet, N. (2009). *L'Analyse de l'eau 9e édition. Entièrement mise à jour*. Dunod.

Salvan, H.M. (1984). Les formations évaporitiques du Trias marocain. Problèmes stratigraphiques, paléogéographiques et paléoclimatologiques. Quelques réflexions. *Revue de Géologie Dynamique et de Géographie Physique*, 25, 87–203.

Seddique, A. A., Masuda, H., Anma, R., Bhattacharya, P., Yokoo, Y., & Shimizu, Y. (2019). Hydrogeochemical and isotopic signatures for the identification of seawater intrusion in the paleobeach aquifer of Cox's Bazar city and its surrounding area, south-east Bangladesh. *Groundwater for Sustainable Development*, 9, 100215. DOI: 10.1016/j.gsd.2019.100215

Sherif, M. M., & Hamza, K. I. (2001). Mitigation of seawater intrusion by pumping brackish water. *Transport in Porous Media*, 43(1), 29–44. DOI: 10.1023/A:1010601208708

Talabi, A. O., Abdu-Raheem, Y. A., Afolagboye, L. O., Oguntuase, M. A., & Akinola, O. O. (2020). Hydrogeochemistry of shallow groundwater in Ado-Ekiti Area, Southwestern Nigeria. *Groundwater for Sustainable Development*, 11, 100386. DOI: 10.1016/j.gsd.2020.100386

Werner, A. D., & Simmons, C. T. (2009). Impact of sea-level rise on sea water intrusion in coastal aquifers. *Groundwater*, 47(2), 197–204. DOI: 10.1111/j.1745-6584.2008.00535.x PMID: 19191886

Xue, H., & Sigg, L. (1999). Comparison of the complexation of Cu and Cd by humic or fulvic acids and by ligands observed in lake waters. *Aquatic Geochemistry*, 5(4), 313–335. DOI: 10.1023/A:1009679819002

Zalidis, G., Stamatiadis, S., Takavakoglou, V., Eskridge, K., & Misopolinos, N. (2002). Impacts of agricultural practices on soil and water quality in the Mediterranean region and proposed assessment methodology. *Agriculture, Ecosystems & Environment*, 88(2), 137–146. DOI: 10.1016/S0167-8809(01)00249-3

Zghibi, A., Merzougui, A., Mansaray, A. S., Mirchi, A., Zouhri, L., Chekirbane, A., Msaddek, M. H., Souissi, D., Mabrouk-El-Asmi, A., & Boufekane, A. (2022). Vulnerability of a Tunisian coastal aquifer to seawater intrusion: Insights from the GALDIT Model. *Water (Basel)*, 14(7), 1177. DOI: 10.3390/w14071177

Index

M

N

O

P

R

S

U

W